COMPUTATIONAL MODELS FOR THE NONLINEAR ANALYSIS OF REINFORCED CONCRETE PLATES

E. Hinton, H.H. Abdel Rahman and M.M. Huq

University College of Swansea

SUMMARY

A finite element computational model for the nonlinear analysis of reinforced concrete solid, stiffened and cellular plates is briefly outlined. Typically, Mindlin elements are used to model the plates whereas eccentric Timoshenko elements are adopted to represent the beams. The layering technique, common in the analysis of reinforced concrete flexural systems, is incorporated in the model.

INTRODUCTION

The present studies were motivated by the need to develop finite element computational models suitable for the efficient and accurate nonlinear analysis of reinforced concrete bridge decks and flexural systems. In particular solid as well as stiffened and cellular plates are of interest and the full load-displacement history is required.

Previous studies have generally been based on Kirchhoff plate and Euler-Bernouilli beam representation and one novel feature of the present studies is the use of Mindlin plate and Timoshenko beam theories. Apart from the fact that transverse shear deformation effects are then automatically taken into account, the use of Mindlin/Timoshenko models allows the adoption of $C^{(o)}$ rather than $C^{(1)}$ finite elements in the discretisation process.

In the nonlinear analysis of reinforced concrete plates it is important to allow for the gradual spread of cracking and yielding of the concrete over the plate thickness as well as the yielding of the steel in the reinforcement. To cater for these effects the well-known layered approach is adopted. Tension stiffening, which will be described later, is included in the concrete model and various unloading curves are considered. As well as providing a better representation of the reinforced concrete behaviour during cracking, tension stiffening appears to have a beneficial effect on the numerical stability of the nonlinear solution scheme.

The authors have successfully experimented with a variety of nonlinear solution schemes. In the present context, experience points to the use of either the Quasi-Newton method with large load increments and a fine convergence tolerance or the initial stiffness method with small load increments and a coarser convergence tolerance. The results quoted here have been obtained using the initial stiffness method with small load increments after

initial cracking has occurred and a coarse convergence tolerance (1%) on the displacements norm.

Also quoted in this paper are results from a numerical experiment with a tentative cellular plate model based on a beam-plate representation. A layered beam models the webs whereas a layered plate with zero rigidity in the void region is used to model the flanges. The transverse shear rigidity of the plate in the plane perpendicular to voids is suitably modified. For cylindrical voids the beams have variable width over the cross-section.

The basic formulation is now described in a little more detail.

BASIC FORMULATION

Main assumptions In Table I the main features of the Mindlin plate formulation are indicated. (NB: The Timoshenko beam formulation, which is based on similar concepts, is omitted.) In the usual Mindlin plate representation integration through the plate thickness is performed explicitly prior to discretisation and therefore the present model is really a degenerated 3D model with restricted (flat) geometry. The main assumption is that normals to the plate midsurface remain straight but not necessarily normal after deformation. Thus the displacements u, v and w at any point in the plate with coordinates (x,y,z) can be expressed as

$$\begin{bmatrix} u(x,y,z) \\ v(x,y,z) \\ w(x,y,z) \end{bmatrix} = \begin{bmatrix} u_o(x,y) - z\,\theta_x(x,y) \\ v_o(x,y) - z\,\theta_y(x,y) \\ w_o(x,y) \end{bmatrix} \qquad (1)$$

where u_o, v_o and w_o are the displacements at the plate midsurface (xy plane) in the x,y and z directions respectively and θ_x and θ_y are the rotations of the normal in the xz and yz planes respectively.

The strain-displacement relationships may therefore be expressed as

$$\underline{\varepsilon} = \begin{bmatrix} \underline{\varepsilon}_m \\ \underline{0} \end{bmatrix} + \begin{bmatrix} z\,\underline{\varepsilon}_f \\ \underline{\varepsilon}_s \end{bmatrix} \qquad (2)$$

in which the membrane strains $\underline{\varepsilon}_m = [u_{o,x},\ v_{o,y},\ u_{o,y} + v_{o,x}]^T$

the flexural strains $\underline{\varepsilon}_f = [-\theta_{x,x},\ -\theta_{y,y},\ -(\theta_{x,y} + \theta_{y,x})]^T$

and the shear strains $\underline{\varepsilon}_s = [w_{o,x} - \theta_x,\ w_{o,y} - \theta_y]^T$

and where $u_{o,x} \equiv \partial u_o / \partial x$ etc.

Elasto-plastic behaviour of concrete Concrete is idealised as an elastic-perfectly plastic material in uniaxial compression. The behaviour of concrete in biaxial stress states is described by an idealised version of the failure envelope obtained by Kupfer et al. (Ref.1). A Von Mises failure surface is used in the biaxial compression zone. See also reference 2. Concrete which has yielded can sustain compressive strains smaller than a limiting strain ε_{cu}. However, when the concrete reaches this strain it is assumed to crush. The crushing surface adopted here is given as

$$c(\underline{\varepsilon}) = \varepsilon_x^2 - \varepsilon_x \varepsilon_y + \varepsilon_y^2 + \frac{3}{4}\gamma_{xy} - \varepsilon_{cu} = 0 \qquad (3)$$

where ε_x and ε_y are the strains in x and y directions and γ_{xy} is the shear strain.

In tension, the concrete is assumed to behave elastically until the tensile strength (f_t') is reached. The concrete then cracks in a direction orthogonal to the stress direction and loses strength. An unloading curve is assumed to account for tension stiffening in the cracked concrete. The stress level in the cracked concrete is interpolated using the tension stiffening curve depending on the degree of straining in the concrete. Concrete cracked in one direction is assumed to have uniaxial properties in that direction only. Concrete cracked in two directions is assumed to lose all of its strength.

The constitutive relations of the concrete are continuously updated according to the stress state in the concrete. However, it must be noted that the shear rigidities always retain their elastic values. The constitutive relations can also be written in partitioned form by separating out the membrane-flexure and shear strain energy terms.

Yielding of steel The steel reinforcement is smeared into steel layers which are assumed to be in a state of uniaxial tension or compression. When the longitudinal stress exceeds the proportionality limit, the steel starts to yield. Strain hardening of the steel can be included if the strain hardening parameter, H' is known. The constitutive relation for yielded steel is given as

$$\sigma_s = \sigma_y + \varepsilon_s E\left[1 - \left(\frac{E}{E+H'}\right)\right] \qquad (4)$$

in which σ_s and ε_s are the stress and strain in steel, E is the Young's Modulus and σ_y is the yield stress.

Slab-beam idealisation The first step in the analysis of a slab-beam system such as the one shown in figure 1 is to discretize the structure into a suitable number of plate and beam elements. In order to simplify the analysis, the stiffeners must be attached along the mesh lines of the plate elements.

The selectively integrated, isoparametric 9-node Heterosis element (Ref.3) is used to model the plate. A hierarchical formulation is adopted to represent all degrees of freedom. Thus the shape functions $\underline{N}_i$ in Table I

are constructed as follows:

$N_1^{(e)}$ ... to $N_8^{(e)}$ are the 8-node Serendipity shape functions and $N_9^{(e)}$ is the bubble shape function $(1-\xi^2)(1-\eta^2)$ associated with the 9^{th} internal node. Note that $\underline{a}_i^{(e)} = [u_i^{(e)}, v_i^{(e)}, w_i^{(e)}, \theta_{xi}^{(e)}, \theta_{yi}^{(e)}]$, $\underline{a}_1^{(e)}$ to $\underline{a}_8^{(e)}$ are the vectors of displacements at nodes 1 to 8 on the boundary of the element and $\underline{a}_9^{(e)}$ is the vector of the degrees of freedom at the hierarchical central node 9. To obtain the displacement vector at node 9 the following expression is used

$$\underline{a}_9' = \sum_{i=1}^{8} \underline{N}_i^{(e)}(0,0)\, \underline{a}_i^{(e)} + \underline{a}_9^{(e)} \qquad (5)$$

The 8-node Serendipity representation can be obtained if all degrees of freedom at node 9 are constrained to zero. If they are all left free, a 9-node Lagrangian representation is obtained. For the Heterosis type representation, only the hierarchical lateral deflection at node 9 is restrained to zero and (5) is used to interpret displacements at node 9.

The 3-node isoparametric Timoshenko beam element is adopted for the beams. The reader should consult reference (4) for further details regarding this element. Beam elements can be located along the mesh lines of the plate elements. The properties of each element are calculated first in the local direction and then transformed to the global coordinate system.

Since the stiffener element is assumed to be monolithically connected to the plate, compatibility of deformation along the junction line between the beam and the plate is enforced since a related system of displacement functions is used for the plate and beam elements. As the details of the stiffness matrix evaluation are standard they are not included here.

The layered beam and plate elements are shown in figure 2.

Nonlinear solution A very small load increment is first applied to the structure, and the cracking load is then estimated. The size of the successive load increments is chosen to be equal to 0.1 times the cracking load as suggested by Johnarry (Ref.5); this improves the rate of convergence since nonlinearities are induced gradually in the structure. For each linearised increment, the unknown displacements are obtained using the initial uncracked stiffness matrix. Strains calculated at the centre of each layer are taken as representative for the whole layer. Stresses are then calculated using the material properties from the previous material state. After checking the state of stress for possible yielding, cracking or crushing, the internal nodal resisting forces can then be calculated and compared with the external forces. The lack of equilibrium between internal and external forces is corrected by applying the out-of-balance or residual forces. The out-of-balance forces are successively applied through a series of iterations of the solution and new corrections to the unknown displacements are obtained until the equilibrium and the constitutive relations are satisfied within a certain allowable limit.

The following convergence criterion is used:

$$(\delta \underline{a}^T \delta \underline{a})^{\frac{1}{2}} / (\underline{a}^T \underline{a})^{\frac{1}{2}} \leq 0.01 \qquad (6)$$

where $\delta \underline{a}$ and $\underline{a}$ are the vectors of iterative and total displacements respectively.

The analysis is terminated when convergence is not achieved within a specified number of iterations. This usually occurs when a structure is about to fail. An estimate of the failure load can then be obtained.

SOLID AND STIFFENED PLATES

Corner supported slab A corner supported doubly reinforced concrete slab (Ref.6) is analysed using a 3x3 mesh in a symmetric quadrant. Initially it is assumed that there is no tension stiffening. Crack patterns on the lower surface of the slab for two load levels (12 kN and 62 kN) are shown in figure 3. Figure 4 shows the load displacement curve. After the steel yields the norm of the out-of-balance membrane forces is rather large even though the displacement convergence tolerance is satisfied. When the displacement tolerance is decreased from 1% to 0.1% after the steel yields, an improved result is obtained as shown in figure 4.

When tension stiffening is used, improved displacement values are obtained. However, this results in higher failure loads. When the unloading part of the tension stiffening curve is extended, better results are obtained for the displacements but the failure loads are still high. When a finer tolerance is used after steel yielding, excellent results are obtained as shown in figure 5.

Stiffened slab The load-central deflection curve predicted by the present model for a reinforced concrete T-beam tested by Cope and Rao (Ref.7) are given in figure 6, which also includes some geometric details of the beam. The load-deflection graphs obtained by Cope and Rao, both experimentally and using a finite element shell formulation, are also reproduced in figure 6. The good agreement between the load-deflection graphs predicted by the present analysis and both Rao's experimental and numerical analyses shows that the proposed approach provides an inexpensive yet fairly accurate analysis for reinforced concrete slabs with RC beam stiffeners.

REINFORCED CONCRETE VOIDED PLATES

Voided reinforced concrete and prestressed concrete plates are widely used for their economic advantages. Although the behaviour of such structures has been studied in the elastic range (Ref.8 , Ref.9), very little experimental and analytical work appears to have been carried out on the behaviour of these structures in the overloading and ultimate stages. In the elastic analysis, equivalent values of the flexural, torsional and shear rigidities of a voided plate can be calculated in different ways (Ref.9 , Ref.10) and used in a finite difference or a finite element analysis of an equivalent orthotropic solid plate. The nonlinear analysis is, however, rather more complex. The spread of plasticity and nonlinearities due to cracking and crushing of concrete

through the depth of the plate must be taken into account. A nonlinear finite element analysis using a 3D or shell formulation to represent different structural elements of the voided plate seems ideal. Unfortunately such a formulation, though feasible, is very expensive. In the present approach, a less expensive approach to the nonlinear analysis of RC voided plates is tentatively suggested. The analysis is based on the formulation of RC stiffened plates described earlier, where the voided plate is assumed to consist of voided plate elements representing the upper and lower flanges and beam stiffeners representing the webs.

The basic assumption is basically that of Mindlin: a transverse plane normal to the middle plane of the plate remains plane but not necessarily normal after deformation, thus implying that the deformations of both flanges are related. This assumption may be justified for voided slabs with large numbers of voids, which have an overall bending behaviour predominantly in the longitudinal direction. In situations where the upper flange is directly loaded by a concentrated load, better results can be achieved if an overlapped mesh is used for a small part around the loaded area to represent the upper flange solely while the original mesh in this part represents the lower flange.

Documented experimental evidence for such structures is provided by Elliott, Clark and Symmons (Ref.11). In this work the results of a quarter scale model reinforced concrete voided bridge have been reported. The geometrical details of the slab are summarised in figure 7. A number of tests were made to study the performance of the slab in the service as well as the over-loading stages and finally an ultimate load test was carried out. This example has been solved using the proposed approach for voided slabs. The discretization and cross section representation of a symmetric quarter of the plate is given in figure 8, while the load-central deflection graphs obtained experimentally and analytically are compared in figure 9. It is reported that the cracking load was nearly equal to the working load which is in agreement with that predicted by the proposed model. The agreement between the experimental and analytical graphs shown in figure 9 is very encouraging. The experimental results show that the slab failed by the formation of a mechanism which involved longitudinal shear/flexural yield lines and transverse hogging flexural yield lines. The analytical study, however, slightly overestimates the failure load since shear failures cannot be predicted by the present model.

CONCLUSIONS

The proposed computational model for the nonlinear analysis of solid and stiffened reinforced plates provides an inexpensive and reasonably accurate approach which can be extended for use with voided plates.

REFERENCES

1. Kupfer, H.; Hilsdorf, H. K, and Rusch, H.: Behaviour of Concrete Under Biaxial Stresses. J. Am. Conc. Inst., Vol.66, No. 8, 1969,pp.656-666.

2. Abdel Rahman, H. H.; Hinton, E.; and Huq, M. M.: Nonlinear Finite Element Analysis of Reinforced Concrete Slab and Slab-beam Structures. Proceedings of Int. Conf. on Numerical Methods for Nonlinear Problems, University College, Swansea, Pineridge Press, 1980, pp. 493-512.

3. Hughes, T.J.R.; and Cohen, M.: The Heterosis Finite Element for Plate Bending, Computers and Structures, vol. 9, 1978, pp. 445-450.

4. Hinton, E.; and Owen, D.R.J.: Finite Element Programming, Academic Press, 1977.

5. Johnarry, T.: Elasto-plastic Analysis of Concrete Structures. Ph.D. Thesis, University of Strathclyde, 1979.

6. Mueller, G.: Numerical Problems in Nonlinear Analysis of Reinforced Concrete. UC-SESM Report No. 77-5, University of California, Sept. 1977.

7. Cope, R. J.; and Rao, P.V.: Nonlinear Finite Element Analysis of Concrete Slab Structures, Proc. Inst. Civ. Engrs., Part 2, vol.63, 1977, pp. 159-179.

8. Hinton, E.; Razzaque, A.; Zienkiewicz, O. C.; and Davies, J. D.: A Simple Finite Element Solution for Plates of Homogeneous, Sandwich and Cellular Construction. Department of Civil Engineering, University of Wales, Swansea, C/R/217/74, 1974.

9. Basu, A. K.; and Dawson, J. M.: Orthotropic Sandwich Plates, Proc. Inst. Civ. Engrs., 1970, Supplementary Paper 7275S, pp. 87-115.

10. Highway Engineering Computer Branch, Department of Transport, User Guide, Slab and Pseudo-slab Bridge Decks, HECB/B1/7.

11. Elliott, G.; Clark, L. A.; and Symmons, R. M.: Test of a Quarter-scale Reinforced Concrete Voided Slab Bridge. Cement and Concrete Association, Dec. 1979, Technical Report 527 (Publication 42.527).

TABLE I.- MINDLIN PLATE FORMULATION

Virtual work equation

$$\int_V \delta \underline{\varepsilon}_1^T \underline{\sigma}_1 \, dV + \int_V \delta \underline{\varepsilon}_2^T \underline{\sigma}_2 \, dV - \int_V \delta \underline{u}^T \underline{b} \, dV - \int_{S_t} \delta \underline{u}^T \underline{t} \, dS = 0$$

where

displacements $\underline{u} = [u, v, w]^T$

virtual displacement $\delta\underline{u} = [\delta u, \delta v, dw]^T$

in-plane strains $\underline{\varepsilon}_1 = [u_{,x}, v_{,y}, u_{,y} + v_{,x}]^T$

$\delta\underline{\varepsilon}_1 = [\delta u_{,x}, dv_{,y}, du_{,y} + dv_{,x}]^T$

shear strains $\underline{\varepsilon}_2 = [w_{,x} - \theta_x, w_{,y} - \theta_y]^T$

$\delta\underline{\varepsilon}_2 = [\delta w_{,x} - \delta\theta_x, \delta w_{,y} - \delta\theta_y]^T$

in-plane stresses $\underline{\sigma}_1 = [\sigma_x, \sigma_y, \tau_{xy}]^T$

$\delta\underline{\sigma}_1 = [\delta\sigma_x, \delta\sigma_y, \delta\tau_{xy}]^T$

shear stresses $\underline{\sigma}_2 = [\tau_{xz}, \tau_{yz}]^T$

$\delta\underline{\sigma}_2 = [\delta\tau_{xz}, \delta\tau_{yz}]^T$

Incremental stress/strain relationships

$$d\underline{\sigma}_1 = \underline{D}_1 \, d\underline{\varepsilon}_1$$

$$d\underline{\sigma}_2 = \underline{D}_2 \, d\underline{\varepsilon}_2$$

Elastic

$$\underline{D}_1 = \underline{D} = \frac{E}{(1-\nu^2)} \begin{bmatrix} 1 & \nu & 0 \\ \nu & 1 & 0 \\ 0 & 0 & \frac{1-\nu}{2} \end{bmatrix}$$

$$\underline{D}_2 = \frac{E}{2(1+\nu)\alpha} \begin{bmatrix} 1 & 0 \\ 0 & 1 \end{bmatrix}$$

α is a modification factor (usually $\alpha = 1.2$)

Plastic

$$\underline{D}_1 = \underline{D} - \underline{D} \left[\frac{\partial F}{\partial \underline{\sigma}_1}\right] \left[\frac{\partial F}{\partial \underline{\sigma}_1}\right]^T \underline{D} \left[\bar{A} + \frac{\partial F}{\partial \underline{\sigma}_1} \underline{D} \frac{\partial F}{\partial \underline{\sigma}_1}\right]^{-1}$$

in which F is the yield function

$F = F(\underline{\sigma}_1, H)$, $\bar{A} = -\frac{1}{\lambda} \frac{\partial F}{\partial H} dH$

λ is the proportionality constraint

H is the hardening parameter

Finite element discretization

$$\underline{u} = \sum_i \underline{N}_i \underline{a}_i$$

$$\underline{\varepsilon}_1 = \sum_i \underline{B}_{1i} \underline{a}_i$$

$$\underline{\varepsilon}_2 = \sum_i \underline{B}_{2i} \underline{a}_i$$

where $\underline{N}_i = N_i \begin{bmatrix} 1 & 0 & 0 & -z & 0 \\ 0 & 1 & 0 & 0 & -z \\ 0 & 0 & 1 & 0 & 0 \end{bmatrix}$

$\underline{a}_i = [u_i, v_i, w_i, \theta_{xi}, \theta_{yi}]^T$

$$\underline{B}_{1i} = \begin{bmatrix} N_{i,x} & 0 & 0 & -zN_{i,x} & 0 \\ 0 & N_{i,y} & 0 & 0 & -zN_{i,y} \\ N_{i,y} & N_{i,x} & 0 & -zN_{i,y} & -zN_{i,x} \end{bmatrix} \qquad \underline{B}_{2i} = \begin{bmatrix} 0 & 0 & N_{i,x} & -N_i & 0 \\ 0 & 0 & N_{i,y} & 0 & -N_i \end{bmatrix}$$

Stiffness Matrices

$$\underline{K}_{ij} = \int_V \underline{B}_{1i}^T \underline{D}_1 \underline{B}_{1j} \, dV + \int_V \underline{B}_{2i}^T \underline{D}_2 \underline{B}_{2j} \, dV$$

Residual forces

$$\underline{\psi}_i = \int_V \underline{B}_{1i}^T \underline{\sigma}_1 \, dV + \int_V \underline{B}_{2i}^T \underline{\sigma}_2 \, dV - \underline{f}_i$$

where the consistent nodal forces $\underline{f}_i = \int_V \underline{N}_i^T \underline{b} \, dV + \int_{S_t} \underline{N}_i^T \bar{\underline{t}} \, dS$

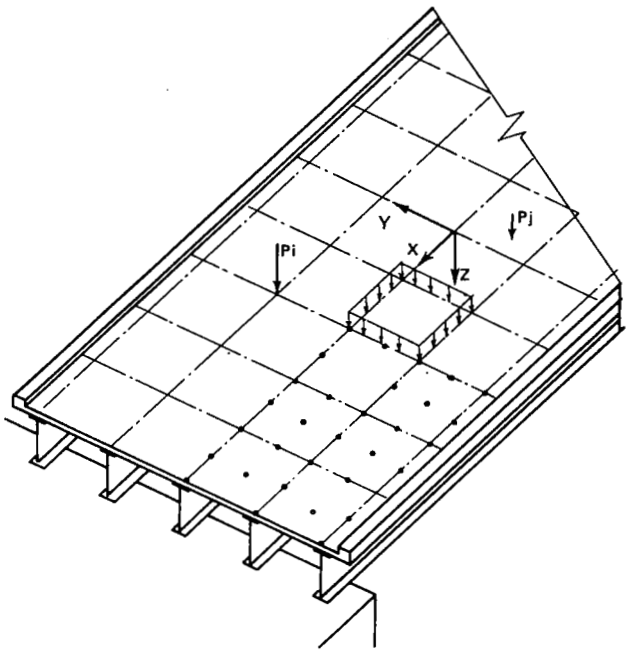

Figure 1.- Typical slab-beam system and its structural idealisation.

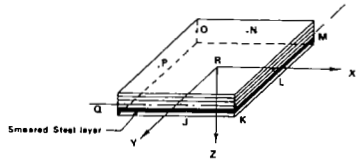

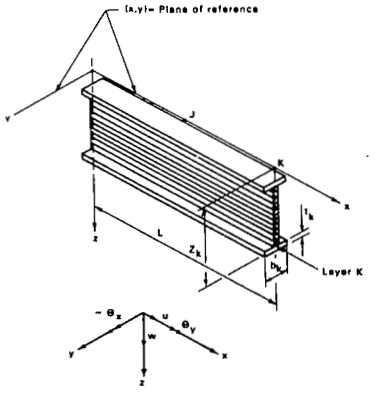

(a) Layered finite plate element.

(b) Layered beam element.

Figure 2.- Layered plate and beam elements.

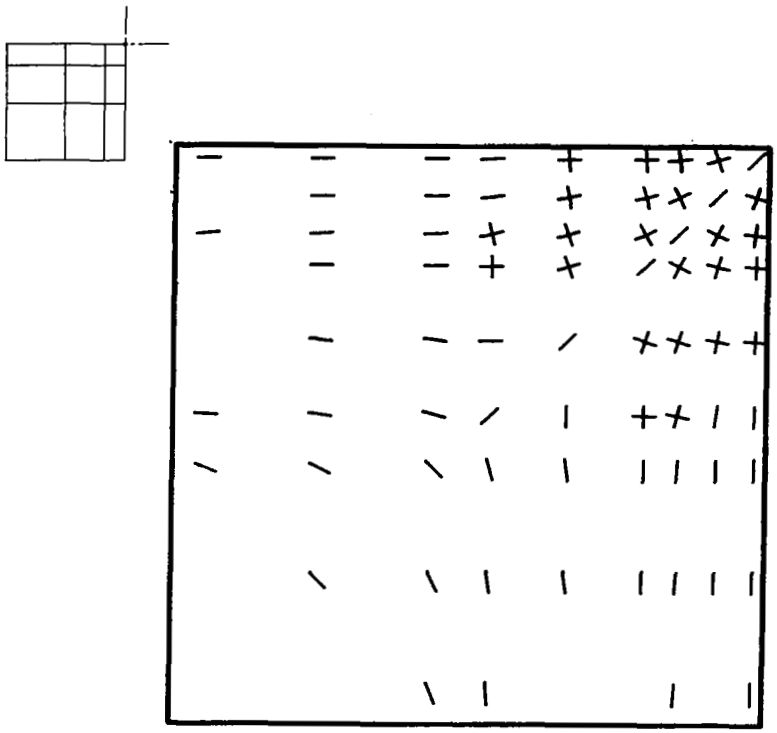

(a) P : 12.0 kN.

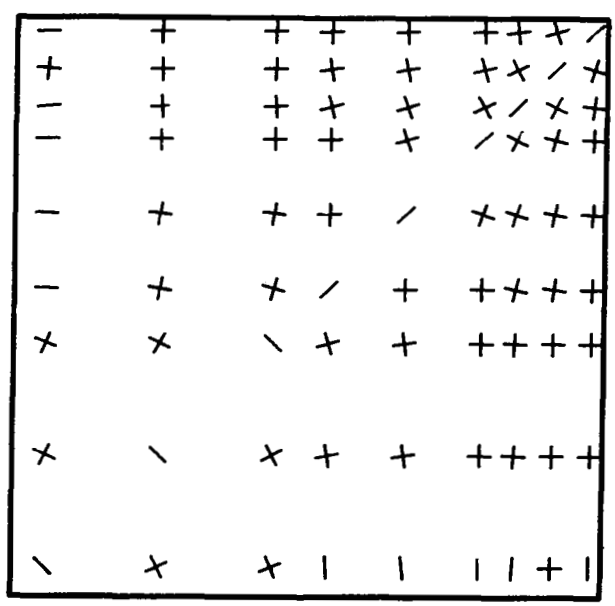

(b) P : 62.0 kN

Figure 3.- Crack patterns on the lower side of Mueller's slab.

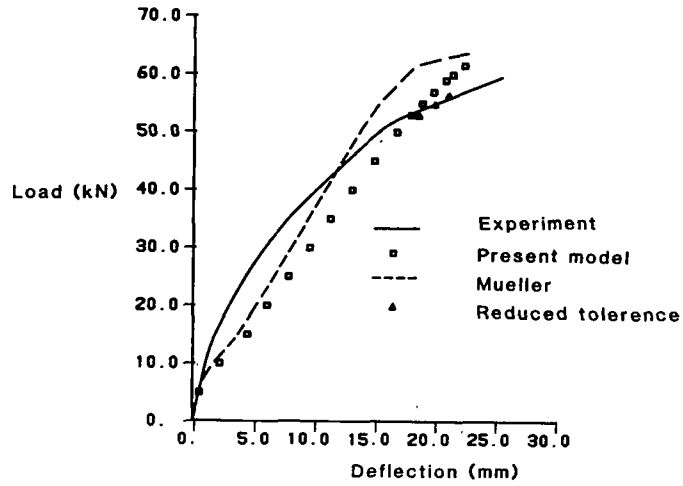

Figure 4.- Load-central deflection curves for Mueller's slab.

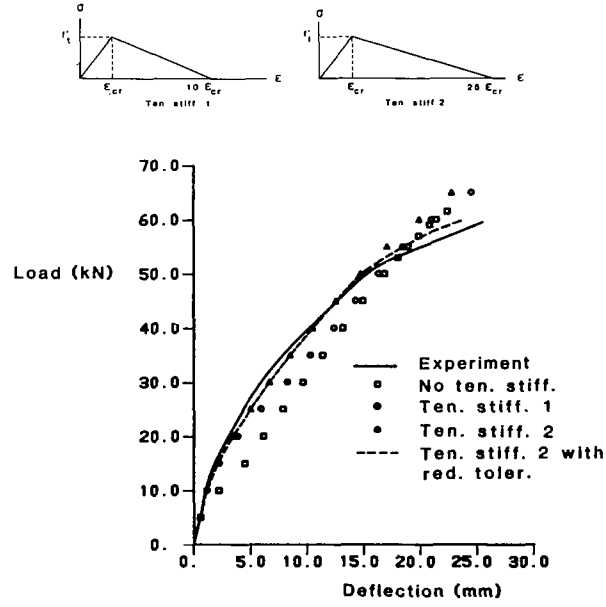

Figure 5.- Effect of tension stiffening on Mueller's slab.

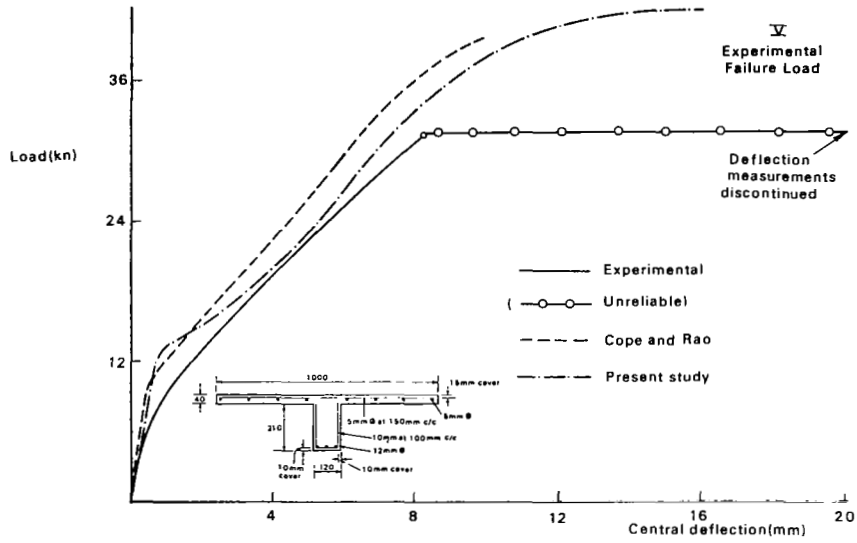

Figure 6.- Load-central deflection curves for T-beam.

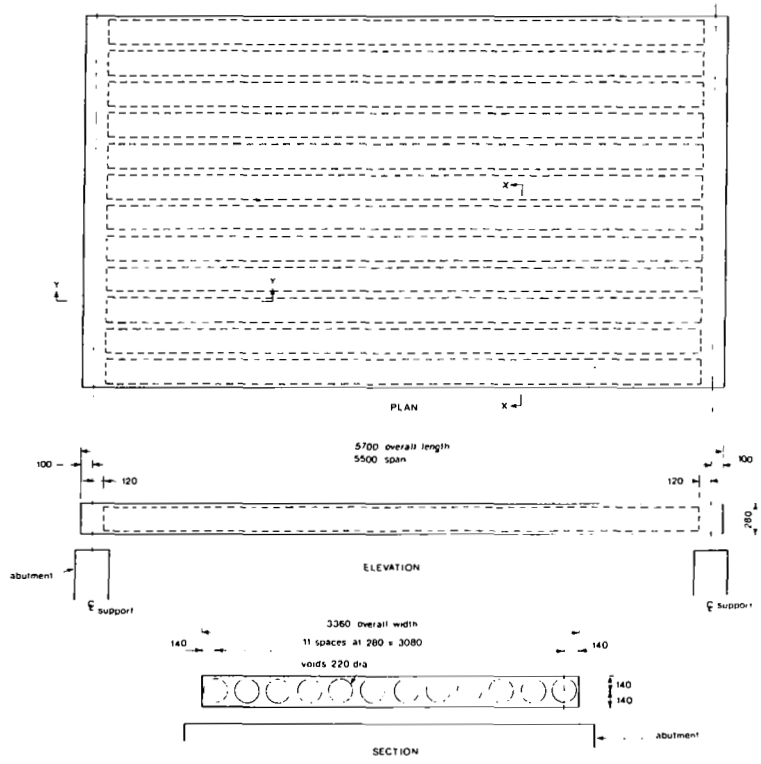

Figure 7.- Details of voided bridge deck model.

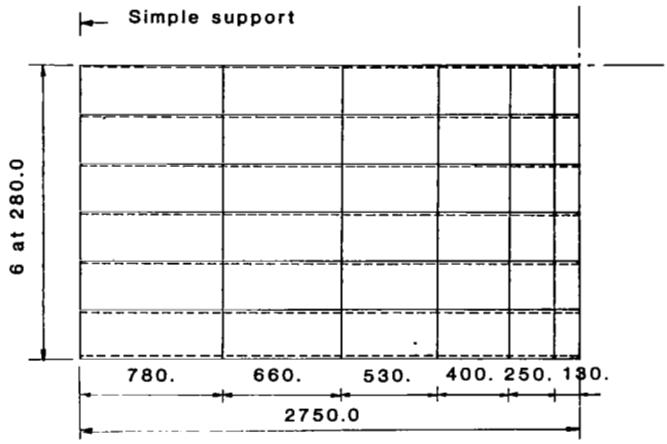

(a) Discretisation of voided plate.

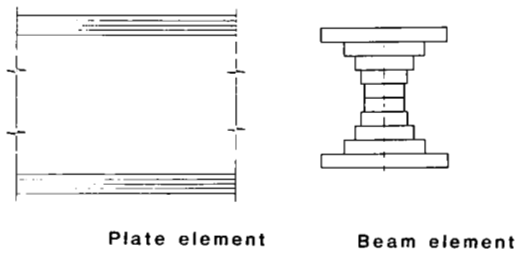

(b) Cross-section representation.

Figure 8.- Finite element discretisation of voided plate.

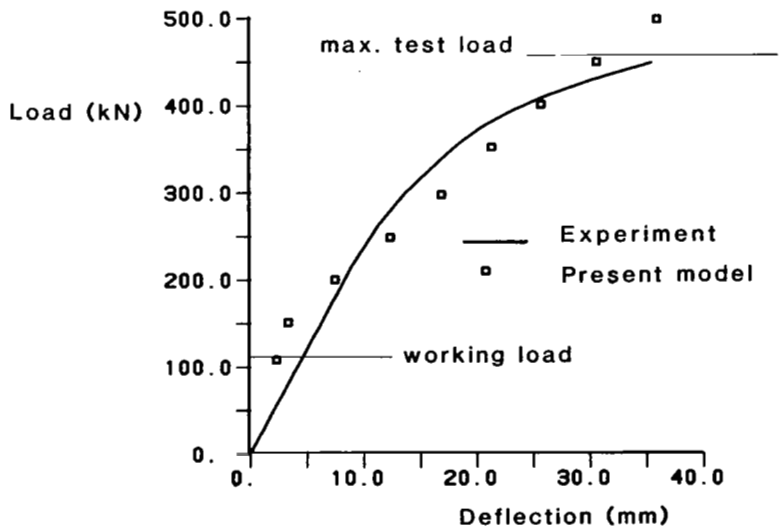

Figure 9.- Load-central deflection curves for voided plate model.